RESEARCH ARTICLE

Macromolecular Rapid Communications
www.mrc-journal.de

The Production of Polysarcosine-Containing Nanoparticles by Ring-Opening Polymerization-Induced Self-Assembly

Anna H. Morrell, Nicholas J. Warren, and Paul D. Thornton**

N-carboxyanhydride ring-opening polymerization-induced self-assembly (NCA ROPISA) offers a convenient route for generating poly(amino acid)-based nanoparticles in a single step, crucially avoiding the need for post-polymerization self-assembly. Most examples of NCA ROPISA make use of a poly(ethylene glycol) (PEG) hydrophilic stabilizing block, however this non-biodegradable, oil-derived polymer may cause an immunological response in some individuals. Alternative water-soluble polymers are therefore highly sought. This work reports the synthesis of wholly poly(amino acid)-based nanoparticles, through the chain-extension of a polysarcosine macroinitiator with L-Phenylalanine-NCA (L-Phe-NCA) and Alanine-NCA (Ala-NCA), via aqueous NCA ROPISA. The resulting polymeric structures comprise of predominantly anisotropic, rod-like nanoparticles, with morphologies primarily influenced by the secondary structure of the hydrophobic poly(amino acid) that enables their formation.

1. Introduction

Polymerization-Induced Self-Assembly (PISA) has emerged over the past decade as a convenient and highly rational method of producing block copolymer nanoparticles with a range of morphologies, including spherical micelles, wormlike micelles and vesicles in addition to more complex structures, such as oligolamellar vesicles, framboidal vesicles and branched worms.[1,2,3–6] Unlike post-polymerization processing methods, such as solvent exchange or thin-film rehydration,[7,8] PISA facilitates synthesis and self-assembly in one-pot, at solid concentrations of up to 50% w/w.[9] This alleviates several issues associated with post-polymerization self-assembly methods such as the requirement for multiple solvents,[8] poor reproducibility, and low concentrations which limit scale-up opportunities.[10]

PISA is most commonly mediated by RAFT polymerization due to its tolerance of a range of reaction conditions and its applicability to a number of different monomer types.[9,11] It can be carried out in non-polar[6,12–18] and polar media,[19–22] including water.[23–27] It is also possible to mediate PISA using other reversible de-activation polymerization techniques (RDRP), including atom transfer radical polymerization (ATRP)[28–30] and nitroxide-mediated polymerization (NMP).[31,32] Additionally, PISA has been reported using several non-radical polymerization methods, including living anionic polymerization,[33,34] ring-opening metathesis polymerization (ROMP)[35–37] and traditional ring-opening polymerization (ROP).[38,39]

Despite its versatility, the preparation of degradable nanoparticles via PISA has been relatively sparse. One common approach involves radical ring-opening polymerization (rROP), which introduces cleavable bonds in the carbon backbone of vinyl polymers through co-polymerization of traditional monomers with cyclic ketene acetals (CKA)[40] and thionolactones.[41,42] These bonds can be hydrolytically degraded to produce low molecular weight vinyl polymers and oligomers. The formation of degradable nanoparticles has also been explored using reverse-sequence RAFT PISA. This avoids some of the complex syntheses of precursor monomers and rate hindrance observed during rROP[43] by using a hydrophobic poly(caprolactone) (PCL) macro-CTA solubilized with a hydrophilic vinyl monomer. These were degraded under mild conditions leaving only the soluble vinyl polymer block.

Another important technique that has recently emerged is PISA mediated by N-carboxyanhydride ring-opening polymerization (NCA ROPISA).[38,39,44–48] This technique provides potential benefits on several fronts: the resulting polymers are not only degradable but owing to their derivation from amino acids – which are endogenous to biological systems – the degradation products are environmentally benign. NCA ROPISA was first explored by Jiang et al. in THF, where PEG-poly(phenylalanine)-based nanoparticles were produced in situ and shown to degrade under enzymatic conditions.[38] From a structural perspective, poly(amino acid)s have a unique ability to adopt

A. H. Morrell, N. J. Warren
School of Chemical and Process Engineering
University of Leeds
Leeds LS2 9JT, UK
E-mail: n.j.warren@leeds.ac.uk
P. D. Thornton
Leeds Institute of Textiles and Colour (LITAC)
School of Design
University of Leeds
Leeds LS2 9JT, UK
E-mail: p.d.thornton@leeds.ac.uk

The ORCID identification number(s) for the author(s) of this article can be found under https://doi.org/10.1002/marc.202400103

DOI: 10.1002/marc.202400103

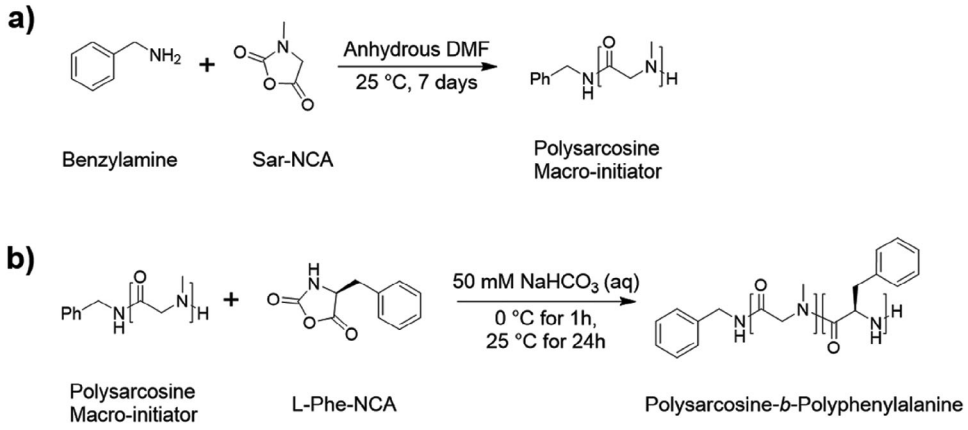

Scheme 1. NCA ROP of a) Sarcosine-NCA in DMF using benzylamine initiator b) Phe-NCA in aqueous solution using a $PSar_{113}$ macro-initiator.

an ordered secondary structure through readily forming hydrogen bonds between polymer chains. Further studies have therefore investigated the factors that determine morphology of nanoparticles produced.[44–46] These have reported that, unlike with more well-established methods of PISA – where nanoparticle morphology is determined by block volume fractions and reaction solid content – morphology and anisotropy are predominantly determined by the poly(amino acid) secondary structure[44,45] and monomer chirality.[46] Despite its recent success, examples of NCA ROPISA are still limited,[38,45–47] particularly in an aqueous environment.[39,44,48] Research commonly features a poly(ethylene glycol) hydrophilic stabilizing block[38,39,44–46,48] which has inherent limitations. These include its non-degradability,[49,50] the possibility of an immune response in some individuals,[49,51,52] and accelerated blood clearance, facilitating build up in the liver and kidneys if used over a prolonged period, or at high dosages.[53,54]

Alternatives to PEG are therefore highly sought, particularly in the production of polymer nanoparticles that may be deployed in vivo. One plausible alternative to PEG is polysarcosine (PSar), a water-soluble polypeptoid that, as a result of methylation at the amide nitrogen atom, is exclusively a hydrogen bond acceptor.[55] Consequently, PSar forms favourable interactions with water and limited interactions to proteins, exhibiting resistance to protein fouling.[55] This leads to comparable aqueous solubility and a similar stealth profile to PEG.[56] However, as sarcosine is an amino acid endogenous to the human body,[50] there are mechanisms suggested for the in vivo degradation of PSar.[55] PSar macro-CTAs have been reported in RAFT PISA[57,58] but were used in the production of nanoparticles containing non-degradable, vinyl-based cores.

Herein, we report a unique example of a wholly poly(amino acid)-based PISA system through the chain extension of a PSar macroinitiator by NCA ROPISA of L-phenylalanine-NCA (Phe-NCA) and L-alanine-NCA (Ala-NCA) resulting in two classes of all-poly(amino acid) nanoparticles: PSar-*b*-$PPhe_x$ and PSar-*b*-$PAla_x$. The self-assembly is investigated, particularly the influence of poly(amino acid) secondary structures on nanoparticle morphology. The structural diversity in the β-structures that the hydrophobic amino acid blocks afford was shown to affect the anisotropy and morphology of the resulting nanostructures, both across classes of nanoparticles and within the same series, highlighting further factors in determining nanoparticle morphology in NCA ROPISA. Importantly, this research also provides an insight into the use of PSar as an alternative to PEG for the ROPISA of NCAs, which has significant implications for biomedical applications.

2. Results and Discussion

2.1. Polysarcosine$_{113}$-*b*-Poly(Phenylalanine)$_x$ Synthesis

Initially, the target PSar-*b*-PPhe block copolymer was synthesized using a two-step protocol (**Scheme 1**) whereby benzylamine was used to initiate the polymerization of Sar-NCA via solution ROP in DMF. This yielded the hydrophilic PSar macroinitiator for subsequent ROPISA. Upon completion, ^{1}H NMR spectroscopy revealed peaks between 7.22 and 7.35 ppm corresponding to the aromatic protons of the benzylamine initiator. Additionally, broad peaks at 2.74–2.96 and 3.92 – 4.35 ppm were present that correspond to the methyl and methylene groups of the sarcosine repeat units, respectively. The average degree of polymerization (DP) of PSar was determined to be 113 by comparing the integral of the benzylamine phenyl group (normalized to 5 protons) and integrating the proton peaks corresponding to the sarcosine repeat units. A narrow monomodal chromatogram was obtained by GPC, with a number average molecular weight (M_n) of 6000 g mol^{-1} and a narrow molar mass dispersity (Đ) of 1.22, which is indicative of a well-controlled NCA ROP.

$PSar_{113}$-NH was then used as the macroinitiator for the ROP of the Phe-NCA in aqueous $NaHCO_3$ solution (pH 8.5, 50 mM) at a total solids concentrations ranging from 3% to 10% w/w, and targeting Phe-NCA DP values ranging from 8 to 33 (Scheme 1b). In all cases, Phe-NCA was initially dispersed as a solid, but as the polymerization proceeded, the volume of solid reduced substantially until a homogeneous solution formed. Polymerization occurs if the NCA is sufficiently well-dispersed upon agitation, enabling the insoluble monomer to react with the solution-phase macroinitiator at their interface. Low levels of monomer may be dissolved at sufficient concentration to facilitate polymerization from the macroinitiator. This contrasts to classical PISA in

Table 1. PSar-*b*-PPhe$_x$ block copolymers obtained by NCA ROPISA at different [M]/[I] ratios and different solid contents.

Copolymer Composition[a)]	Target DP	Solids / %	M_n[b)] / g mol^{-1}	Đ[b)]	D_h[c)] / nm	PDI[c)]
PSar$_{113}$ Macroinitiator	N/A	N/A	6000	1.22	N/A	N/A
PSar$_{113}$-*b*-PPhe$_5$	8	3	8800	1.13	100	0.26
PSar$_{113}$-*b*-PPhe$_{13}$	16	3	9800	1.14	109	0.22
PSar$_{113}$-*b*-PPhe$_{21}$	25	3	10 300	1.13	150	0.20
PSar$_{113}$-*b*-PPhe$_{20}$	33	3	10 400	1.10	250	0.28
PSar$_{113}$-*b*-PPhe$_{14}$	16	5	10 000	1.13	95	0.28
PSar$_{113}$-*b*-PPhe$_{17}$	16	10	9400	1.14	118	0.17

[a)] Copolymer composition determined by ^{1}H NMR spectroscopy; [b)] M_n and Đ determined by GPC, in DMF + 1 mg mL^{-1} LiBr, using PMMA standards; [c)] Hydrodynamic diameter and polydispersity index determined using DLS.

which the monomer used for chain extension typically has good solubility.[9]

Carrying out the polymerization in basic solution at reduced temperatures was necessary to retard the rate of NCA hydrolysis, which leads to uncontrolled polymerization and side reactions[59,60] that have higher activation energies relative to chain propagation.[59,61]

According to ^{1}H NMR spectroscopy, the resulting PSar$_{113}$-*b*-PPhe$_x$ block copolymers had DP values ranging from 5 to 21 for the Phe block (**Table 1**). The ^{1}H NMR spectra were indicative of successful polymerizations, exhibiting minimal presence of remaining NCA, and broadened multiplet resonances attributable to the nitrogen, phenyl and methylene protons of the PPhe block at 8.07 – 8.5, 7.12 – 7.20, and 4.49 – 4.5 ppm, respectively (**Figure 1**). This was also confirmed by ^{13}C NMR spectroscopy and FTIR analysis. The ^{13}C NMR spectrum revealed the loss of CO_2 during the polymerization through the absence of a peak at 151 ppm, which corresponds to the N—C═O group of Phe-NCA. FTIR analysis showed the replacement of the Phe-NCA anhydride bands, at ≈1845 and 1770 cm^{-1}, with an amide I band originating from the polymer at 1630 cm^{-1}. Monomodal chromatograms were obtained for the block copolymers which shifted to lower retention times, relative to that of the corresponding PSar macroinitiator (**Figure 2**). This confirmed block extension. GPC also revealed relatively narrow molar mass dispersity values, ranging from 1.10 to 1.13 (Table 1).

^{1}H NMR spectroscopy and GPC were also used to determine DP and average polymer M_n values, respectively. For the block copolymer samples targeting DPs of 8 to 25, prepared at 3% w/w solids, both ^{1}H NMR spectroscopy and GPC analyses reported an increase in the DP and M_n in line with the upward trend in monomer-to-initiator ratio ([M]/[I]) albeit with values slightly below the target DP of 25 Phe repeat units, whereby PSar$_{113}$-*b*-PPhe$_{21}$ was produced. Following this, a stagnation in DP and M_n occurred as a block copolymer of PSar$_{113}$-*b*-PPhe$_{20}$ was produced, with a comparable M_n to that of PSar$_{113}$-*b*-PPhe$_{21}$, despite targeting eight additional Phe repeat units. It is likely that this stagnation in DP is a consequence of a combination of reasons including the stable secondary structure formed by the PPhe block, and the chemical and geometrical restrictions that the Phe side chains pose. Grazon et al. reported that for ROPISA to be successful, micelles must form during growth of the short diblock polymers which are capable of preferentially accommodating unreacted monomer.[39] These act as a locus to facilitate further polymerization in a similar manner to RAFT mediated PISA.[23] The insolubility of Phe-NCA in aqueous solution likely led to slow diffusion of the remaining insoluble monomers within the reaction media. Additionally, although nanoparticles are formed at relatively short block lengths compared to copolymers that do not feature hydrogen bond donor and acceptor groups, the propensity to form secondary structures may have also impeded further monomer ingress to the growing polymer chain end, resulting in an upper limit to the core DP. The Phe residues pack very tightly due to their hydrophobic nature[62] and the phenyl R group participates in multiple non-bonded interactions which significantly stabilizes secondary structures.[63,64] Any late stage monomer diffusing into the core may have been blocked from reaching the growing polymer end by the secondary structure network produced by the PPhe block, along with the possible formation of hydrogen bonds by the unreacted NCA itself. Additionally, the R groups of any unreacted NCAs close to the polymer extremity may form weak hydrogen bonds reducing the nucleophilicity of the amine chain end.[60] In contrast to traditional PISA,[4,6,9] where monomer preferentially moves to the core, the monomer becomes increasingly excluded from the secondary polypeptide structure which forms within the particles. This results in the stagnation in polymerization, limiting further particle growth or morphology evolution. Such factors may affect the extent of NCA ROPISA, emphasising the importance of amino acid selection when designing these copolymers.

Following successful polymer synthesis, the production of nanostructures formed in situ during Phe-NCA polymerization was probed. To the best of our knowledge, nanostructure creation would signal the first report of ROPISA using PSar as the stabilizing block to form block copolymer nano-objects consisting solely of amino acid repeat units. DLS studies revealed that for syntheses conducted at 3% solids content, the sphere-equivalent z-average diameter (D_h) of the nano-objects increased systematically with respect to target DP, from 100 nm up to 250 nm with polydispersity index (PDI) values ranging from 0.20 to 0.28 (Figure S5a, Supporting Information). Whilst expected for PSar-*b*-PPhe$_{5\text{-}21,}$ which have increasing M_n values according to GPC, the difference in D_h of 100 nm between PSar-*b*-PPhe$_{21}$ and PSar-*b*-PPhe$_{20}$ is perhaps surprising. These block copolymers have very similar average DP and M_n values (Table 1), and therefore comparable D_h values are expected,

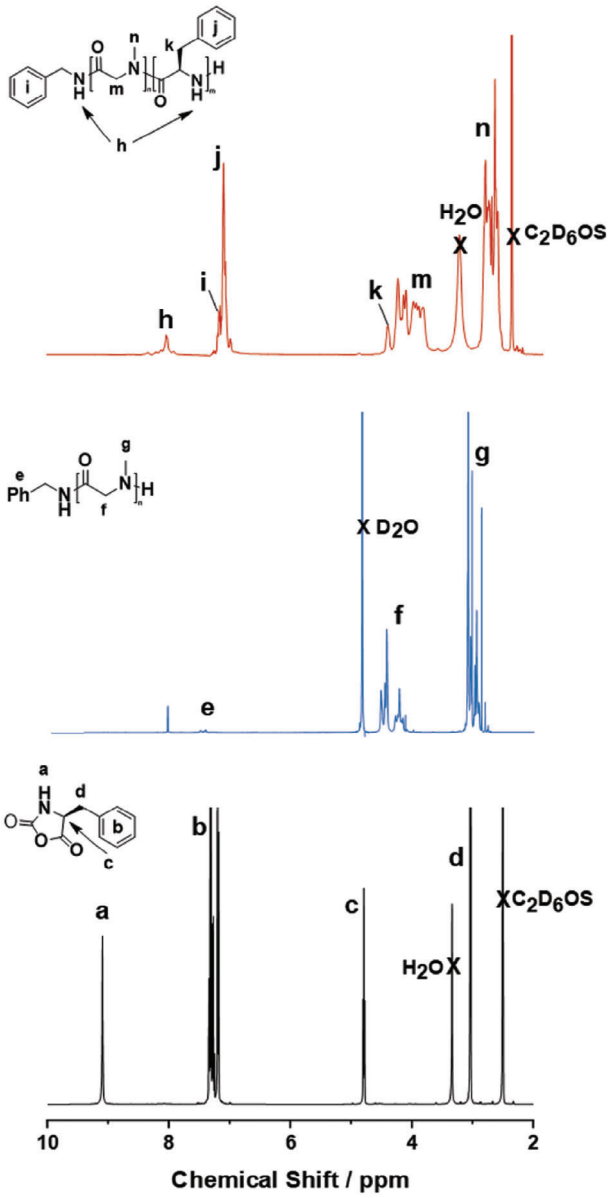

Figure 1. ^{1}H NMR spectra of Phe-NCA, the PSar macro-initiator, and PSar$_{113}$-*b*-PPhe$_{16}$, illustrating the loss of resonances attributable to Phe-NCA and indicating successful PPhe synthesis. Spectra obtained at 400 MHz using DMSO-d6 and D_2O.

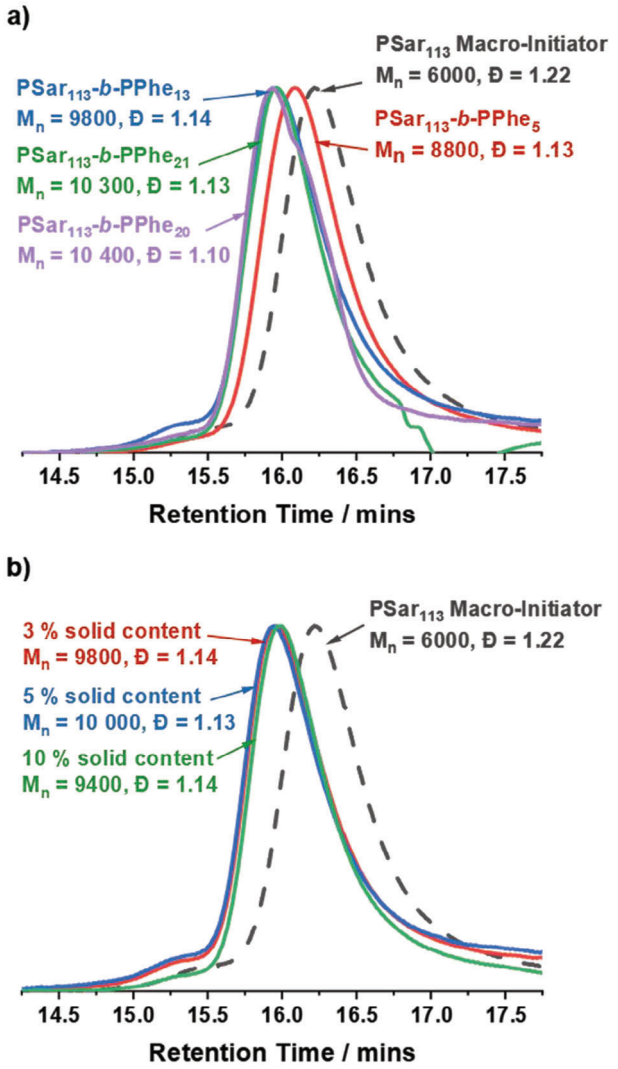

Figure 2. GPC traces showing the chain extension of PSar$_{113}$ with Phe repeat units for samples, a) produced at 3% solid content with varying PPhe lengths, and b) produced at varying solid contents with a PPhe [M]/[I] of 16.

suggesting there may be morphological differences between the samples. Direct analysis by TEM is therefore necessary as DLS provides a sphere-equivalent z-average diameter and caution in data interpretation must be practiced with non-spherical particles. Actual particle physical dimensions and the hydrodynamic diameter reported by DLS analysis likely vary owing to differences in the rotational and translational diffusion coefficients of spherical and non-spherical particles. However, such data provides evidence of the presence of nanoparticles and a comparative indication of nanoparticle sizes prior to their direct analysis by Transmission Electron Microscopy (TEM).

TEM analysis (**Figure 3**) highlighted that all samples contained non-spherical aggregates which included both isolated and clustered anisotropic nanostructures. However, there was a noticeable morphological difference between the samples of PSar-*b*-PPhe$_{5\text{-}21}$ and PSar-*b*-PPhe$_{20}$; the latter sample contained more elongated and plate-like nanostructures.

Secondary structure has been reported as a factor in determining the nanoparticle morphology produced in aqueous NCA ROPISA when exploring morphological differences between polymers with different poly(amino acid) blocks.[44] As a result, the type of secondary structure present in the block copolymers was determined, using FTIR spectroscopy and circular dichroism (CD) (**Figure 4**), to assess if this may cause morphological differences in samples with the same poly(amino acid) block too. In particular, the amide I band in the FTIR spectrum was monitored as the positioning of this band is dependent on the type of secondary structure present. The amide I bands for

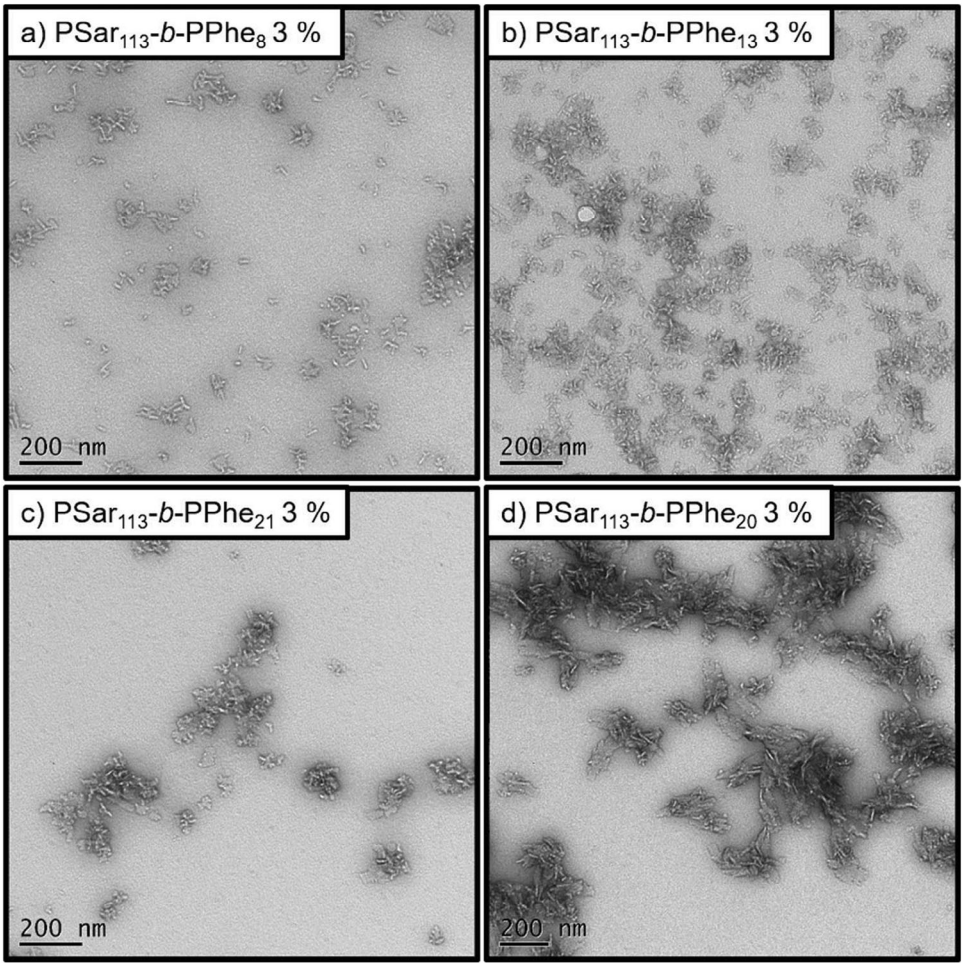

Figure 3. TEM images displaying the anisotropic nanostructures for $PSar_{113}$-*b*-$PPhe_x$, produced at 3 w/w % (scale bar = 200 nm).

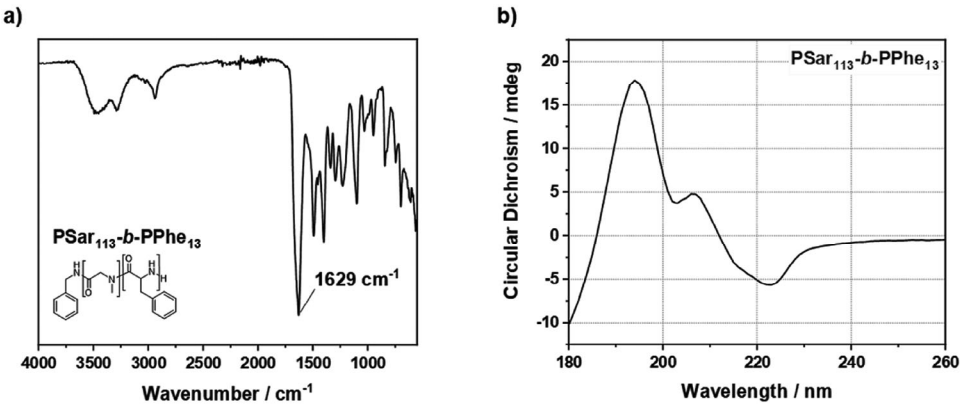

Figure 4. a) FTIR spectrum displaying an amide I band at 1633 cm^{-1}, in line with the expected value for poly(amide)s exhibiting β-sheet secondary structure, and b) CD spectrum of $PSar_{113}$-*b*-$PPhe_{13}$, exhibiting a curve characteristic of β-sheets.

random coils and α-helices are present at 1656 and 1650 cm^{-1}, respectively, whereas for β-sheets, a characteristic signal is found at 1630 cm^{-1}.[65]

As discussed previously, in all cases an amide I band was present at 1630 cm^{-1}. This alludes to the presence of beta sheets, expected in phenylalanine-containing poly(amino acids) due to their bulky phenyl pendant groups.[66,67] Additionally, the CD spectra obtained are all indicative of structures made up of predominantly β-structures, with a positive band at ≈195 nm and a broad negative band at ≈220 nm in all cases.[68] However,

Table 2. Percentages of different β-structures present in nanoparticles, produced by NCA ROPISA at different [M]/[I] ratios and solid contents, using either Phe-NCA or Ala-NCA as the monomer.

Copolymer Composition	Solids / %	Anti-parallel β-sheets[a] / %	Parallel β-sheets[a)] / %	β-turns[a)] / %	Others[a)] / %
$PSar_{113}$-*b*-$PPhe_5$	3	20.4	12.1	13.9	53.1
$PSar_{113}$-*b*-$PPhe_{13}$	3	26.1	17.8	0.7	55.3
$PSar_{113}$-*b*-$PPhe_{21}$	3	44.4	7.1	0	48.5
$PSar_{113}$-*b*-$PPhe_{20}$	3	33.4	66	0	0
$PSar_{113}$-*b*-$PPhe_{14}$	5	12.2	25.7	14.8	47.3
$PSar_{113}$-*b*-$PPhe_{17}$	10	31.6	4.1	16.3	48.1
$PSar_{96}$-b-$PAla_7$	10	27.4	12.1	8.7	48
$PSar_{96}$-b-$PAla_{15}$	10	81.5	18.5	0	0
$PSar_{96}$-b-$PAla_{23}$	10	93.1	6.9	0	0
$PSar_{96}$-b-$PAla_{32}$	10	100	0	0	0

[a)] Determined using circular dichroism followed by β-structure selection (BeStSel), a secondary structure selection method.

clear differences in the CD spectra of PSar-*b*-$PPhe_{5\text{-}21}$ and PSar-*b*-$PPhe_{20}$ were found. In particular, the former three samples exhibited an additional, smaller peak at ≈205 nm that was indistinct in PSar-*b*-$PPhe_{20}$. Spectral diversity across samples of β-structure rich macromolecules is not unusual in CD spectroscopy as there is a large amount of structural diversity in β-sheets, due to variation in their orientation and twisting.[69] Quantitative analysis was therefore carried out using β-structure selection (BeStSel), a secondary structure estimation method that takes into account the twist of β-structures,[69] to investigate the presence of different types of β-structures across the samples (**Table 2**). The samples of PSar-*b*-$PPhe_{5\text{-}21}$ exhibited mixtures of anti-parallel and parallel sheets, along with turns and other structures such as β-bridges, bends and loops. Conversely, PSar-*b*-$PPhe_{20}$ exhibited only anti-parallel and parallel sheets. This difference likely causes the observed morphological differences across samples, although is unexpected given that PSar-*b*-$PPhe_{21}$ and PSar-*b*-$PPhe_{20}$ possess comparable DP and M_n values. The change in morphology must therefore be linked to the increased amount of monomer present during the polymerization. The ^{1}H NMR spectra of all samples exhibit some evidence of a very small amount of unreacted monomer, wherein there is a small peak at ≈5 ppm attributable to the methylene proton in Phe-NCA. Despite being present in all samples, error within NMR analysis prevented sufficient characterization to quantify the amount of unreacted monomer remaining in each sample. It can however be assumed that because PSar-*b*-$PPhe_{20}$ has the largest discrepancy between target and actual DP, the largest quantity of unreacted monomer most likely remains. Some of this unreacted monomer may have entered the micellar core but been unable to reach the growing polymer chain end. The R groups of NCAs can form hydrogen bonds which may have interacted with the PPhe polymer and other unreacted monomer, altering the overall secondary structure of the PPhe block.[70] Whilst it is likely this also occurred to some extent with the other samples of PSar-*b*-$PPhe_x$, PSar-*b*-$PPhe_{20}$ contained the largest quantity of unreacted monomer, resulting in more pronounced secondary structure disruption and alteration to the nano-object dimensions.

Synthesis of block copolymers with a DP of 16 at higher solid contents of 5 and 10% were also attempted, which successfully yielded nanoparticles comprising $PSar_{113}$-*b*-$PPhe_{14}$ and $PSar_{113}$-*b*-$PPhe_{17}$, respectively. Both samples had similar M_n and Đ values (Table 1 and Figure 2b) to those produced at 3% solid content indicating that this synthesis can be successfully carried out at higher concentrations. Additionally, DLS reported the formation of nanoparticles at 5% and 10% solids. These exhibited only a small variation in hydrodynamic diameter, increasing from 95 to 118 nm, with associated PDI values between 0.17 and 0.26, as expected for block copolymers of comparable lengths (Figure S5b, Supporting Information).

DLS was also used to assess the stability of selected nanoparticles, with equivalent DPs at different solid contents, stored in aqueous suspensions at room temperature after 12 months (Figure S7, Supporting Information). The nanoparticles all exhibited comparable sizes to their initial D_h with PDI values that, importantly, remained consistently relatively low. This suggests that polymer aggregation had not taken place, and that the particles, at this targeted DP, are stable in aqueous solvent for at least one year.

2.2. Polysarcosine$_{96}$-*b*-Poly(Alanine)$_x$ Synthesis

To assess the versatility of using Psar as the stabilizing hydrophilic block in NCA ROPISA, polyalanine (PAla) was grafted from the Psar macroinitiator in aqueous solution. PAla is an excellent candidate to drive stable nanoparticle formation during ROPISA owing to the extensive hydrogen bond interactions that form between PAla chains. The secondary structures that form between poly(amino acids), such as α-helices and β-sheets, and the type of structure adopted by the polymers is dependent on the amino acids present in the polymer. Work carried out by both Grazon et al., and Li et al., reported this to have an effect on the anisotropy and aspect ratio of the nanoparticles produced through the PEG_x-NH_2 NCA ROPISAs of BLG-NCA and Leu-NCA, and Phe-NCA, respectively.[44,46]

Table 3. PSar-*b*-PAla$_x$ block copolymers obtained by NCA ROPISA at different [M]/[I] ratios.

Copolymer Composition[a)]	Target DP	Solids / %	D_h[b)] / nm	PDI[b)]	Mean Length[c)] / nm
$PSar_{96}$ Macroinitiator	N/A	N/A	N/A	N/A	N/A
$PSar_{96}$-*b*-$PAla_7$	8	10	243	0.26	90 ± 31
$PSar_{96}$-*b*-$PAla_{15}$	16	10	113	0.38	65 ± 17
$PSar_{96}$-*b*-$PAla_{23}$	25	10	260	0.32	88 ± 24
$PSar_{96}$-*b*-$PAla_{32}$	33	10	262	0.29	82 ± 26

[a)] Copolymer composition determined by ^{1}H NMR spectroscopy; [b)] Hydrodynamic diameter and polydispersity index determined using DLS; [c)] Mean length determined by measuring 50 nanoparticles on TEM images.

Consequently, morphologies of nanostructures formed from poly(amino acids) are dependent not just on block length, as per standard polymer synthesis, but also from secondary structure contributions. As a result, we explored the NCA ROPISA of Ala-NCA.

$PSar_{96}$ was used to initiate a series of polymerizations with target Ala DPs of 8, 16, 25, and 33 at 10% w/w. Extensive intramolecular hydrogen bonds between PAla chains ensures that even a relatively small number of Ala repeat units can instigate and maintain stable nanoparticle formation, a key feature of poly(amino acids)-based nanoparticles in general. According to ^{1}H NMR spectroscopy, a series of copolymers were produced with DP values comparable to the target values (**Table 3**). In this case, no stagnation in DP was observed. This could be attributed to the greater conformational flexibility in PAla secondary structures, due to the small size of the methyl side chain, relative to PPhe.[71] More unreacted monomer is therefore able to reach the polymer extremity over the course of the reaction. M_n and dispersity analyses of these polymers by GPC were challenging because of poor polymer solubility in commonly used organic solvents, owing to the strong intra-chain hydrogen bonding that takes place between PAla chains. However, the abilities of $PSar_{96}$-*b*-$PAla_x$ to form nanoparticles in aqueous solution could still be explored.

DLS analysis confirmed the presence of nanoparticles in all cases (Figure S6, Supporting Information) with sphere-equivalent z-average diameters ranging from 113 to 262 nm and PDI values of 0.26 to 0.38 (Table 3). Nanoparticle size did not increase systematically though, with similar sizes for $PSar_{96}$-*b*-$PAla_x$, where x is 7, 23, or 32, but a D_h of 113 nm when x is 15. TEM analysis revealed narrow, worm-like nanostructures (**Figure 5**) in all cases suggesting that a difference in morphology between samples was not the cause of this unusual DLS trend, as per $PSar_{113}$-*b*-$PPhe_x$. The images produced by TEM did however highlight the presence of large aggregates in the $Psar_{96}$-*b*-$PAla_7$ sample, not obvious in the other samples, and upon measuring the lengths of the nanoparticles exhibited in each sample, $Psar_{96}$-*b*-$PAla_{15}$ was shown to have the shortest mean length (Table 3). Despite this, there was much less variation in the sizes across samples measured by TEM compared to DLS measurement. This may be the result of incompatibilities between DLS analysis and non-spherical nanoparticles, as the PDI values are also higher than expected. Again, although DLS provides a guide to the size and any trends that are present in non-spherical nanoparticle samples, direct nanoparticle analysis by TEM is required to accurately determine the nanoparticle distribution.

TEM analysis was also extremely useful in highlighting the difference in morphology exhibited by $PSar_{96}$-*b*-$PAla_x$ relative to the PPhe-based nanostructures. FTIR analysis and CD spectroscopy were carried out to determine the secondary structures present in these nanoparticles (**Figure 6**) and assess if morphological differences across the two nanoparticle classes is a consequence of variation in the polymer secondary structure. FTIR exhibited an amide I band at ≈1630 cm^{-1} alluding to the presence of β-structures in all cases, and CD confirmed this with characteristic β-structure bands exhibited at ≈195 and ≈220 nm. The peak at ≈206 nm, present in most of the spectra for PSar-*b*-$PPhe_x$ samples, was not exhibited in the PSar-*b*-$PAla_x$ samples though. As noted previously, this is not unusual in the CD spectra of β-structure rich proteins. BeStSel was therefore used to quantify the β-structure diversity within the samples of PSar-*b*-$PAla_x$, and relative to the samples of PSar-*b*-$PPhe_x$ (Table 2). PSar-*b*-$PAla_7$ was found to have a mixture of anti-parallel and parallel sheets, turns and other structures, such as loops and bridges, which is expected because sequences shorter than 10 Ala units produce minimal β-sheet formation, ensuring that secondary structure with limited definition forms.[72–74] From PSar-*b*-$PAla_{15}$ onward, the nanoparticles exhibit exclusively anti-parallel and parallel β-sheets with the percentage of anti-parallel structures increasing up to 100%, as the PAla block increases in length. In addition, this quantification confirmed the differences in β-structures present between PSar-*b*-$PPhe_x$ and PSar-*b*-$PAla_x$ which is most likely causes the difference in morphology across the samples. This difference is expected as the two amino acids have different R groups of different steric properties and capability to form non-bonded interactions, leading to secondary structures with differing levels of conformational flexibility.

3. Conclusions

ROPISA to create nanoparticles consisting of amphiphilic block copolymers that contain solely amino acid repeat units is reported for the first time. PSar acts as an effective macroinitiator and stabilizing block to facilitate in situ nanoparticle formation during polymerization in aqueous solution. Polymeric nanostructures created from $PSar_{113}$-*b*-$PPhe_x$ were anisotropic with many possessing rod-like structures maintained by β-sheets formed by hydrogen bonds between adjacent PPhe blocks.

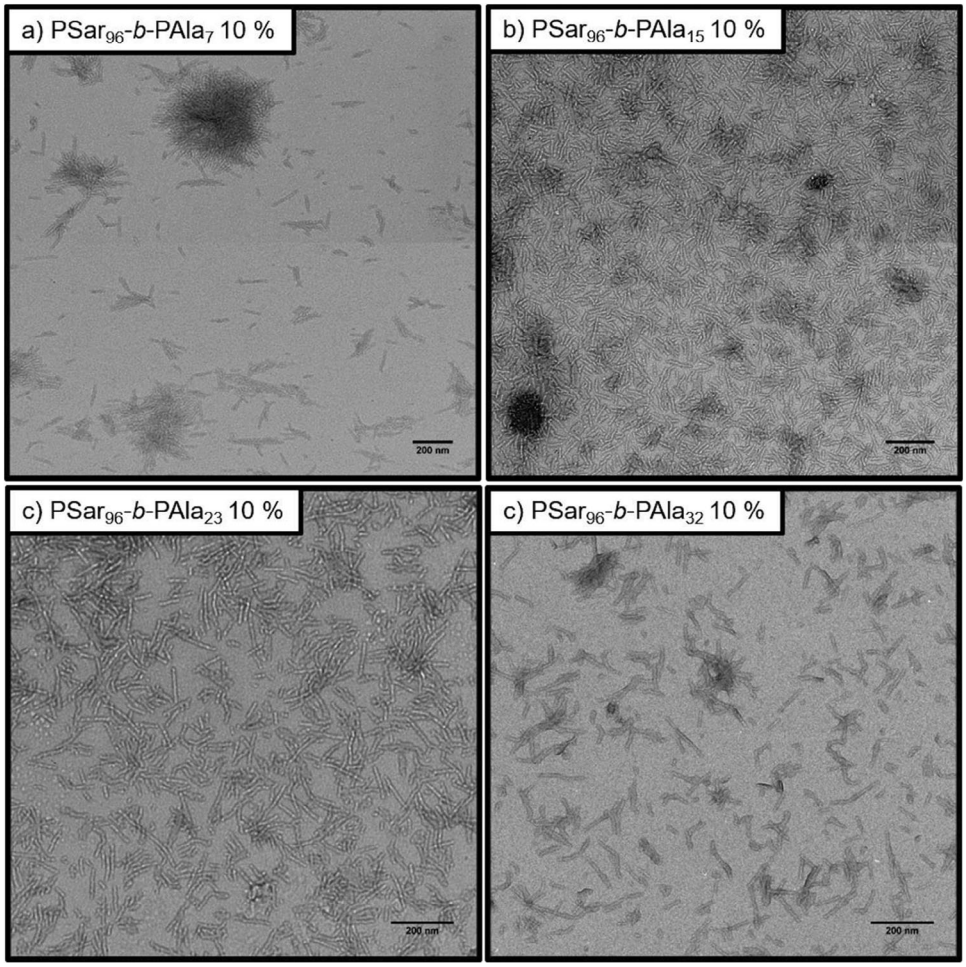

Figure 5. TEM images displaying the rod-like nanoparticles and plate-like aggregates for $PSar_{96}$-*b*-$PAla_x$, produced at 10 w/w % (scale bar = 200 nm).

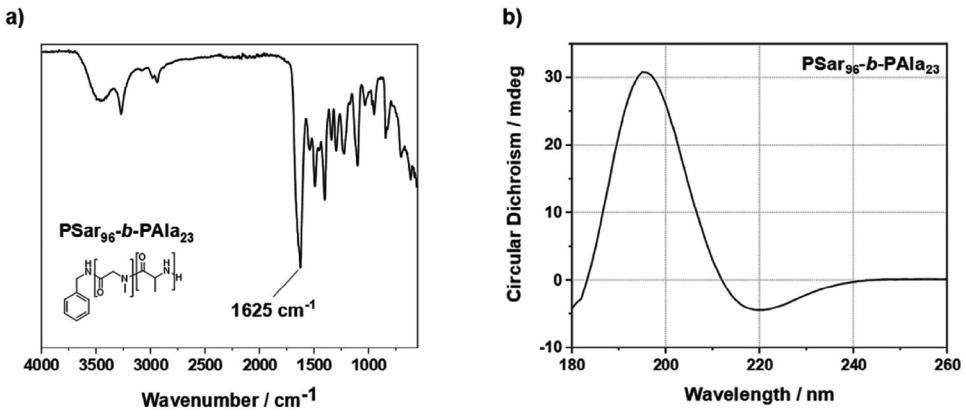

Figure 6. a) FTIR spectrum of $PSar_{96}$-*b*-$PAla_{23}$ exhibiting an amide I band at 1625 cm^{-1} characteristic of β-sheets and b) associated CD spectrum alluding to a β-sheet secondary structure.

Differences in morphologies were exhibited across the series, which was found to be a result of diversity within the β-structures formed by the PPhe blocks, possibly resulting from the presence of unreacted NCA. Significantly, such nanostructures remained stable in aqueous solution for at least 12 months. The versatility of PSar to act as an effective macroinitiator and stabilizing block for ROPISA was further demonstrated by the polymerization of a second amino acid NCA, Ala-NCA, yielding PSar-*b*-$PAla_x$. Narrow nano-objects were produced, with worm-like character, which differed from the PSar-*b*-$PPhe_x$ structures

produced. PAla-containing polymers formed β-structures but the types of these differed from those produced by PPhe-containing polymers. In turn, this affects the morphologies of the nanostructures formed. The amino acid selected for chain extension may therefore be altered to affect the morphologies of exclusively poly(amino acid) nanostructures formed by ROPISA.

Supporting Information

Supporting Information is available from the Wiley Online Library or from the author.

Acknowledgements

This research was supported through a studentship supported by the EPSRC Centre for Doctoral Training in Molecules to Product (EP/SO22473/1). The authors thank G. Nasir Khan for help with CD measurements.

Conflict Of Interest

The authors declare no conflict of interest.

Author Contributions

A.H.M: Conception, Investigation, Formal analysis, Writing (original draft preparation, review & editing) P.D.T: Conception, Supervision, Writing, Review, & Editing N.J.W: Conception, Supervision, Writing, Review & Editing.

Data Availability Statement

The data that support the findings of this study are available from the corresponding author upon reasonable request.

Keywords

amino acids, aqueous ring-opening polymerization, nanoparticles, polymer morphology and secondary structure, polymerization-induced self-assembly

Received: February 26, 2024
Revised: April 2, 2024
Published online: April 10, 2024

[1] N. J. Warren, O. O. Mykhaylyk, D. Mahmood, A. J. Ryan, S. P. Armes, *J. Am. Chem. Soc.* **2014**, *136*, 1023.
[2] C. J. Mable, L. A. Fielding, M. J. Derry, O. O. Mykhaylyk, P. Chambon, S. P. Armes, *Chem. Sci.* **2018**, *9*, 1454.
[3] A. Blanazs, A. J. Ryan, S. P. Armes, *Macromolecules* **2012**, *45*, 5099.
[4] S. L. Canning, G. N. Smith, S. P. Armes, *Macromolecules* **2016**, *49*, 1985.
[5] L. Qiu, X. Han, C. Xing, U. Glebe, *Small* **2023**, *19*, 2207457.
[6] C. György, S. P. Armes, *Angew. Chem.* **2023**, *62*, e202308372.
[7] Y. Zhu, B. Yang, S. Chen, J. Du, *Prog. Polym. Sci.* **2017**, *64*, 1.
[8] Q. Gu, H. Li, E. J. Cornel, J. Du, *Cell Rep. Phys. Sci.* **2023**, *4*, 101495.
[9] N. J. W. Penfold, J. Yeow, C. Boyer, S. P. Armes, *ACS Macro Lett.* **2019**, *8*, 1029.
[10] Z. Zhao, S. Lei, M. Zeng, M. Huo, *Aggregate* **2024**, *5*, e418.
[11] C. Liu, C.-Y. Hong, C.-Y. Pan, *Polym. Chem.* **2020**, *11*, 3673.
[12] L. A. Fielding, J. A. Lane, M. J. Derry, O. O. Mykhaylyk, S. P. Armes, *J. Am. Chem. Soc.* **2014**, *136*, 5790.
[13] M. J. Derry, L. A. Fielding, S. P. Armes, *Polym. Chem.* **2015**, *6*, 3054.
[14] A. P. Lopez-Oliva, N. J. Warren, A. Rajkumar, O. O. Mykhaylyk, M. J. Derry, K. E. B. Doncom, M. J. Rymaruk, S. P. Armes, *Macromolecules* **2015**, *48*, 3547.
[15] E. J. Cornel, S. van Meurs, T. Smith, P. S. O'Hora, S. P. In Armes, *J. Am. Chem. Soc.* **2018**, *140*, 12980.
[16] E. J. Cornel, P. S. O'Hora, T. Smith, D. J. Growney, O. O. Mykhaylyk, S. P. Armes, *Chem. Sci.* **2020**, *11*, 4312.
[17] C. György, S. J. Hunter, C. Girou, M. J. Derry, S. P. Armes, *Polym. Chem.* **2020**, *11*, 4579.
[18] R. R. Gibson, A. Fernyhough, O. M. Musa, S. P. Armes, *Polym. Chem.* **2021**, *12*, 2165.
[19] E. R. Jones, M. Semsarilar, A. Blanazs, S. P. Armes, *Macromolecules* **2012**, *45*, 5091.
[20] M. Semsarilar, E. R. Jones, A. Blanazs, S. P. Armes, *Advanced Materials* **2012**, *24*, 3378.
[21] Y. Pei, A. B. Lowe, *Polym. Chem.* **2014**, *5*, 2342.
[22] M. J. Rymaruk, C. T. O'Brien, S. L. Brown, C. N. Williams, S. P. Armes, *Macromolecules* **2020**, *53*, 1785.
[23] A. Blanazs, J. Madsen, G. Battaglia, A. J. Ryan, S. P. Armes, *J. Am. Chem. Soc.* **2011**, *133*, 16581.
[24] Y. Jiang, N. Xu, J. Han, Q. Yu, L. Guo, P. Gao, X. Lu, Y. J. P. C. Cai, *Polym. Chem.* **2015**, *6*, 4955.
[25] S. J. Byard, M. Williams, B. E. McKenzie, A. Blanazs, S. P. Armes, *Macromolecules* **2017**, *50*, 1482.
[26] E. E. Brotherton, F. L. Hatton, A. A. Cockram, M. J. Derry, A. Czajka, E. J. Cornel, P. D. Topham, O. O. Mykhaylyk, S. P. Armes, *J. Am. Chem. Soc.* **2019**, *141*, 13664.
[27] T. J. Neal, N. J. W. Penfold, S. P. Armes, *Angew. Chem.* **2022**, *61*, e202207376.
[28] S. Sugihara, S. P. Armes, A. L. Lewis, *Angew. Chem.* **2010**, *49*, 3500.
[29] A. Alzahrani, D. Zhou, R. P. Kuchel, P. B. Zetterlund, F. Aldabbagh, *Polym. Chem.* **2019**, *10*, 2658.
[30] A. Shahrokhinia, R. A. Scanga, P. Biswas, J. F. Reuther, *Macromolecules* **2021**, *54*, 1441.
[31] G. Delaittre, M. Save, B. Charleux, *Macro Molecular* **2007**, *28*, 1528.
[32] X. G. Qiao, P. Y. Dugas, B. Charleux, M. Lansalot, E. Bourgeat-Lami, *Macromolecules* **2015**, *48*, 545.
[33] J. Wang, M. Cao, P. Zhou, G. Wang, *Macromolecules* **2020**, *53*, 3157.
[34] C. Zhou, J. Wang, P. Zhou, G. Wang, *Polym. Chem.* **2020**, *11*, 2635.
[35] D. B. Wright, M. P. Thompson, M. A. Touve, A. S. Carlini, N. C. Gianneschi, *Macro Molecular* **2019**, *40*, 1800467.
[36] D. B. Wright, M. A. Touve, M. P. Thompson, N. C. Gianneschi, *ACS Macro Lett.* **2018**, *7*, 401.
[37] D. B. Wright, M. A. Touve, L. Adamiak, N. C. Gianneschi, *ACS Macro Lett.* **2017**, *6*, 925.
[38] J. Jiang, X. Zhang, Z. Fan, J. Du, *ACS Macro Lett.* **2019**, *8*, 1216.
[39] C. Grazon, P. Salas-Ambrosio, E. Ibarboure, A. Buol, E. Garanger, M. W. Grinstaff, S. Lecommandoux, C. Bonduelle, *Angew. Chem., Int. Ed. Engl.* **2020**, *59*, 622.
[40] E. Guégain, C. Zhu, E. Giovanardi, J. Nicolas, *Macromolecules* **2019**, *52*, 3612.
[41] M. Lages, N. Gil, P. Galanopoulo, J. Mougin, C. Lefay, Y. Guillaneuf, M. Lansalot, F. D'Agosto, J. Nicolas, *Macromolecules* **2022**, *55*, 9790.

[42] P. Galanopoulo, N. Gil, D. Gigmes, C. Lefay, Y. Guillaneuf, M. Lages, J. Nicolas, F. D'Agosto, M. Lansalot, *Angew. Chem., Int. Ed. Engl.* **2023**, *62*, 202302093.
[43] M. A. H. Farmer, O. M. Musa, S. P. Armes, *Angew. Chem., Int. Ed. Engl.* **2023**, *62*, 202309526.
[44] C. Grazon, P. Salas-Ambrosio, S. Antoine, E. Ibarboure, O. Sandre, A. J. Clulow, B. J. Boyd, M. W. Grinstaff, S. Lecommandoux, C. Bonduelle, *Polym. Chem.* **2021**, *12*, 6242.
[45] A. Duro-Castano, L. Rodríguez-Arco, L. Ruiz-Pérez, C. De Pace, G. Marchello, C. Noble-Jesus, G. Battaglia, *Biomacromolecules* **2021**, *22*, 5052.
[46] H. Li, E. J. Cornel, Z. Fan, J. Du, *Chem. Sci.* **2022**, *13*, 14179.
[47] F. Yang, Z. Liu, W. Si, Z. Song, L. Yin, H. Tang, *ACS Macro Lett.* **2022**, *11*, 663.
[48] S. X. Huang, Z. H. Wang, M. Lin, X. H. Fu, J. Sun, *Polym. Chem.* **2023**, *14*, 1801.
[49] R. P. Garay, R. El-Gewely, J. K. Armstrong, G. Garratty, P. Richette, *Expert Opin. Drug Delivery* **2012**, *9*, 1319.
[50] Y. Hu, Y. Hou, H. Wang, H. Lu, *Bioconjugate Chem.* **2018**, *29*, 2232.
[51] L. Dézsi, T. Mészáros, G. Kozma, M. H. Velkei, C. Z. Oláh, M. Szabó, Z. Patkó, T. Fülöp, M. Hennies, M. Szebeni, B. A. Barta, B. Merkely, T. Radovits, J. Szebeni, *GeroScience* **2022**, *44*, 597.
[52] Y. Deng, T. Zou, X. Tao, V. Semetey, S. Trepout, S. Marco, J. Ling, M.-H. Li, *Biomacromolecules* **2015**, *16*, 3265.
[53] T. Ishida, M. Harada, X. Y. Wang, M. Ichihara, K. Irimura, H. Kiwada, *J. Controlled Release* **2005**, *105*, 305.
[54] S. S. Nogueira, A. Schlegel, K. Maxeiner, B. Weber, M. Barz, M. A. Schroer, C. E. Blanchet, D. I. Svergun, S. Ramishetti, D. Peer, P. Langguth, U. Sahin, H. Haas, *ACS Appl. Nano Mater.* **2020**, *3*, 10634.
[55] A. Birke, J. Ling, M. Barz, *Prog. Polym. Sci.* **2018**, *81*, 163.
[56] D. Huesmann, A. Sevenich, B. Weber, M. Barz, *Polymer* **2015**, *67*, 240.
[57] S. Varlas, P. G. Georgiou, P. Bilalis, J. R. Jones, N. Hadjichristidis, R. K. O'Reilly, *Biomacromolecules* **2018**, *19*, 4453.
[58] H. Yu, N. Ingram, J. V. Rowley, S. Parkinson, D. C. Green, N. J. Warren, P. D. Thornton, *J. Mater. Chem. B* **2019**, *7*, 4217.
[59] W. Vayaboury, O. Giani, H. Cottet, A. Deratani, F. Schué, *Macromol. Rapid Commun.* **2004**, *25*, 1221.
[60] G. J. M. Habraken, K. H. R. M. Wilsens, C. E. Koning, A. Heise, *Polym. Chem.* **2011**, *2*, 1322.
[61] H. Cao, J. Yao, Z. Shao, *Polym. Int.* **2012**, *61*, 774.
[62] K. M. Makwana, R. Mahalakshmi, *Protein Sci.* **2015**, *24*, 1920.
[63] N. Y. Palermo, J. Csontos, R. F. Murphy, S. Lovas, *Int. J. Quantum Chem.* **2008**, *108*, 814.
[64] E. Lanzarotti, R. R. Biekofsky, D. A. Estrin, M. A. Marti, A. G. Turjanski, *J. Chem. Inf. Model.* **2011**, *51*, 1623.
[65] T. A. Bauer, J. Imschweiler, C. Muhl, B. Weber, M. Barz, *Biomacromolecules* **2021**, *22*, 2171.
[66] H. R. Kricheldorf, D. Müller, J. Stulz, *Makromol. Chem.* **1983**, *184*, 1407.
[67] N. Judge, D. Pavlović, E. Moldenhauer, P. Clarke, R. Brannigan, A. Heise, *Polym. Chem.* **2022**, *13*, 2822.
[68] V. I. Dodero, Z. B. Quirolo, M. A. Sequeira, *Front. Biosci. (Landmark Ed)*. **2011**, *16*, 61.
[69] A. Micsonai, F. Wien, L. Kernya, Y.-H. Lee, Y. Goto, M. Réfrégiers, J. Kardos, *Proc. Natl. Acad. Sci. USA* **2015**, *112*, E3095.
[70] R. Lumry, H. Eyring, *J. Phys. Chem.* **1954**, *58*, 110.
[71] K. A. Henzler Wildman, D. K. Lee, A. Ramamoorthy, *Biopolymers* **2002**, *64*, 246.
[72] M. Rinaudo, A. Domard, *J. Am. Chem. Soc.* **1976**, *98*, 6360.
[73] P. J. Baker, K. Numata, *Biomacromolecules* **2012**, *13*, 947.
[74] S. E. Blondelle, B. Forood, R. A. Houghten, E. Pérez-Payá, *Biochemistry* **1997**, *36*, 8393.

